other hallmarks of infection. Furthermore, geographical clustering of patients is a strongly suggestive factor for infectious diseases.

In 2005, we encountered a patient with severe early-onset dementia. Histopathology of biopsied brain tissue revealed encephalitis. The putative pathogen was cell wall deficient and exhibited several unreported features. In the following 7 years, we treated 3 additional patients presenting with similar clinical symptoms and pathologic findings. All patients inhabited towns located on a peninsula of Kyushu Island, Japan. Here we describe the clinical, pathologic, and radiologic findings of this disease and report results of genomic screening for preliminary identification of the causative pathogen.

METHODS **Patient 1.** The first patient presenting with this unique form of encephalomyelitis was a 47-year-old man from a fishing town on Kyushu Island. Three months before admission, he started eating excessively. His speech and daily activities decreased for a few weeks, accompanied by memory disturbance and disorientation. Two physicians made an initial diagnosis of Alzheimer disease. No abnormalities were observed on blood analyses or MRI during the first 3 months after onset; however, from the fourth month, elevated CSF cell count was observed and fluid-attenuated inversion recovery (FLAIR) MRI revealed high signal intensity regions in the dorsal pons, bilateral insular cortex, and subcortical temporal region (figure 1, A–C). Neurologic examination revealed severe disorientation, loss of calculation, and memory

| Figure 1 | Initial brain imaging |

(A–C) patient 1; (D–F) patient 2; (G–I) patient 3; (J–L) patient 4; and (M) patient 2. Brain fluid-attenuated inversion recovery (FLAIR) MRI performed on admission (A–C) revealed abnormally high intensity at the dorsal pons, bilateral insular cortex, and subcortical region in patient 1. According to FLAIR MRI, patient 2 and patient 4 had similar brain lesions, including abnormalities around the inferior horn of the lateral ventricle (D, J) and diffuse high intensity in the deep white matter of the frontotemporoparietal regions (E, K). These lesions are mainly confined to the white matter, as revealed by the relative sparing of the cortex, and are enhanced by gadolinium administration in T1-weighted MRI (F, L). In contrast, FLAIR MRI of patient 3 revealed patchy lesions in the subcortical area of the left temporal lobe (G) and in the basal ganglion (H). Contrast-enhanced FLAIR MRI revealed hyperintense lesions along the left central sulcus (I). Sagittal T2-weighted images depict an inhomogeneously hyperintense spinal cord, stretching from the cervico-occipital junction to the thoracic cord region (M).

Table 1 Initial evaluation of 4 patients with progressive dementia

	Patient 1	Patient 2	Patient 3	Patient 4
Age, y/sex	47/male	72/female	57/female	70/female
Onset age, y	47	70	56	68
Main symptoms	Dementia	Dementia/semicoma	Dementia	Dementia
	Myoclonus	Parkinsonism	Parkinsonism	Frontal lobe dysfunction
		Pyramidal symptoms	Psychosis	Cerebellar ataxia
Tongue involuntary movement	Dystonia	Unknown	Tremor	Dyskinesia
Initial diagnosis	Alzheimer disease	IVL	Panic disorder	Unknown dementia
Time from onset to treatment with TMP-SMX, mo	11	20	12	27
Effect of high-dose TMP-SMX + steroid	Definitely improved	Initially improved[a]	Moderately improved	Initially improved[a]
Prognosis	Recovered	Slowly progressive	Recovered	Died
Immunologic test	Negative	Negative	CSF IL-6 elevated	CSF IL-6 elevated
			Antiribosomal P+	
HDS-R	9	13	17	12
MMSE	NE	14	NE	18
MRI abnormalities	Subcortex	Subcortex	Subcortex	Subcortex
	Insular cortex	Deep white matter	Basal ganglion	Deep white matter
	Pons	Spinal cord	Arachnoid membrane of parietal lobe	
CSF analysis				
White blood cells, /mm³ (RV: 0–5)	27	64	63	7
Protein, mg/dL (RV: 15–40)	78	66.24	74	45
Glucose, mg/dL, CSF/serum	46/102	47/142	56/123	59/129

Abbreviations: IL = interleukin; IVL = intravascular lymphoma; HDS-R = Revised Hasegawa Dementia Scale (max score 30); MMSE = Mini-Mental State Examination (max score 30); NE = not examined; RV = reference value; TMP-SMX = trimethoprim/sulfamethoxazole.
[a] Treatment was not maintained because of liver failure induced by high-dose TMP-SMX.

All patients exhibited hypointensities on FLAIR images, and the lesions were slightly enhanced by gadolinium. These lesions were spread throughout the brain but were particularly noticeable in the subcortical white matter of the temporal lobe. The cortex, basal ganglia, brainstem, and spinal cord could be involved at more advanced stages (figure 1). These abnormalities also improved with TMP-SMX and prednisolone combination therapy (figure e-1).
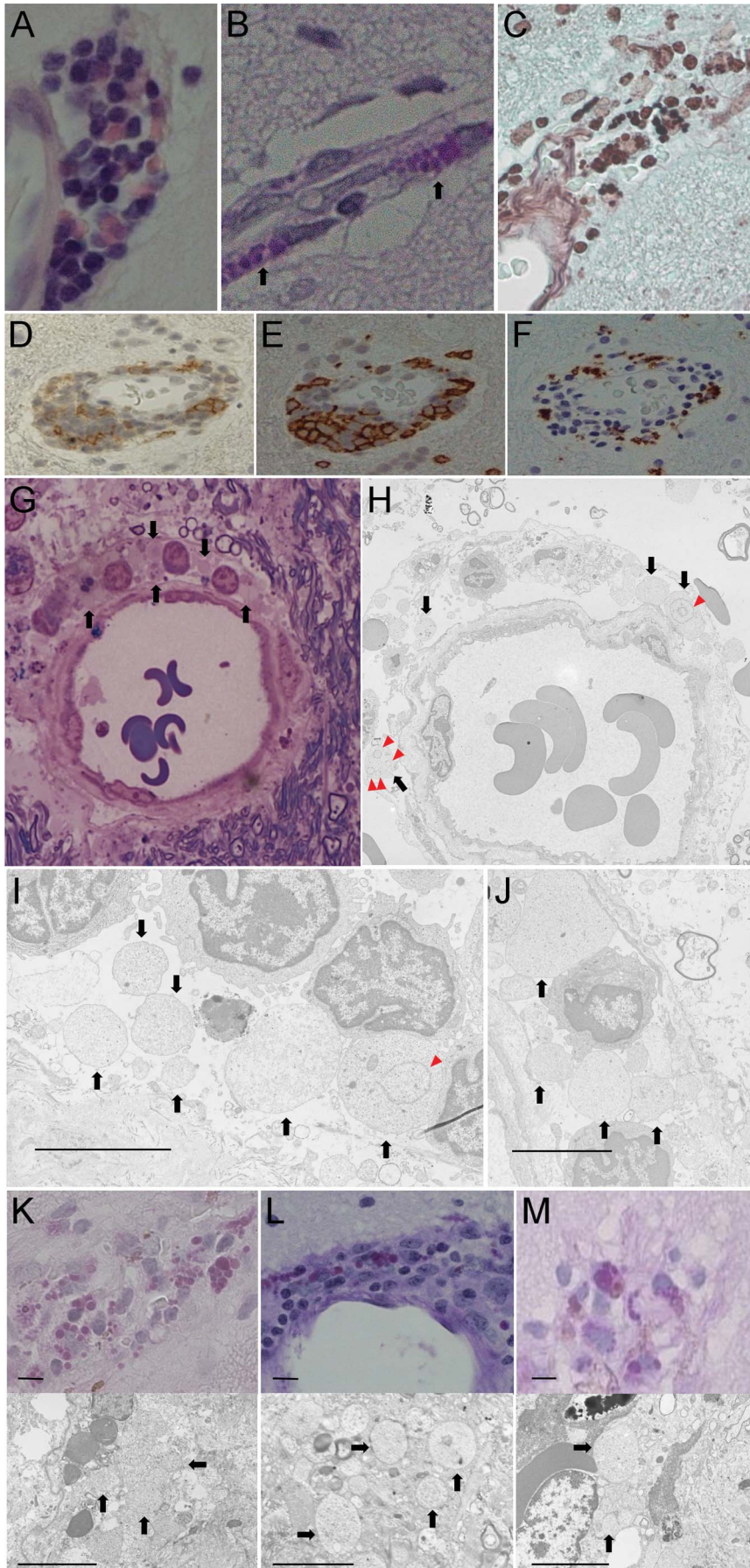
Histopathology. Brain tissue samples from the 4 patients showed comparable histopathologic changes consisting of perivascular spongiosis and infiltration of mononuclear cells (figure 2, E and F). Subcortical changes were more prominent than cortical changes, and there was slight white matter gliosis. No aggregates of foamy macrophages were seen, but microabscess formation was observed in patient 3. Moreover, infiltration of inflammatory cells was observed in the subarachnoid space. No significant necrosis, hemorrhage, neuronophagia, or demyelination was found.

No pathogen was identified in H&E-stained sections, but PAS staining revealed round- to oval-shaped bodies (2–7 μm in diameter) in the extracellular area and cytoplasm of macrophages infiltrating the perivascular region (figure 2, B, K–M). Part of these structures morphologically resembled Michaelis-Gutmann bodies. These bodies were positive for Grocott stain (figure 2C) but negative for Gram stain and immunostaining against toxoplasma antigen. Electron microscopy revealed that these bodies were anuclear cells of irregular shape and varying size. They lacked a nuclear membrane and cell wall but showed occasional cytoplasmic structures (figure 2, H–J).

Genomic analysis and gene sequence–based analysis using 16S/18S rRNA. No amplicon products of bacterial, fungal, protozoal, or archaeal origin were obtained from CSF or brain tissue DNA using previously described universal primer pairs targeting 16S/18S rRNA.

Pathogen detection by unbiased next-generation sequencing and nested PCR. Among 7,292,715 DNA fragments obtained from patient 3, 130 reads showed a striking homology to Halobacteriaceae (domain Archaea) under

Figure 2 Histochemical and immunohistochemical staining and electron microscopic examination of structures in the brain biopsy

Hematoxylin & eosin staining (A), periodic acid-Schiff (PAS) staining (B), and Grocott staining (C) of brain biopsy samples show the presence of round pathogens, similar to Michaelis-Gutmann bodies, located mainly around the blood vessels. Some CD4-positive T lymphocytes are also located around the vessels (D). CD8-positive T lymphocytes appear to be the main invasive cells (E), whereas CD68-positive macrophages are only present in patches (F). Toluidine blue and Safranin O stain of Epon-embedded semithin sections show some pathogens without nuclei around vessels (G). Electron microscopy (H–J) shows an irregular shape of pathogens (diameter 2–7 μm) without cell walls and nuclei (arrows) but with some membranous structures in the cytoplasm (triangles). Scale bar = 5 μm. Brain biopsies from patients 2 (K), 3 (L), and 4 (M) demonstrate a similar histopathology to that of patient 1, with 2–7 μm round PAS-positive pathogens located mainly around the vessels. The agents showed an irregular shape with no detectable cell wall or nucleus under an electron microscope (arrows). Scale bar = 5 μm.
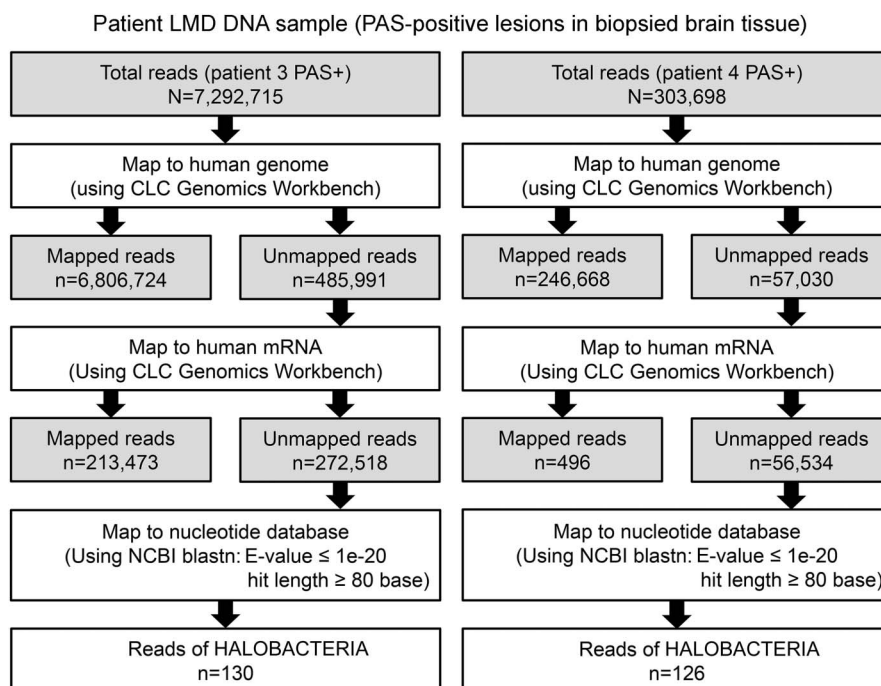
conditions E-value $<1e^{-20}$, hit length >80, and identity $>70\%$ (figure 3, table e-3). These sequences were not substantially homologous to known bacteria or eukarya sequences (E-value $> 1e^3$). Moreover, of 303,698 DNA fragments isolated from patient 4, 126 reads also showed a high degree of homology with Halobacteria, particularly *Halorubrum lacusprofundi* and *Halophilic archaeon* (figure 3, table e-3). In contrast, genomic DNA extracted from brain tissues of patients with papillary meningioma (4,760,858 reads), intravascular lymphomatosis (5,259,934 reads), or glioblastoma (5,027,830 reads) showed no significant homology to known archaeal genomic or mRNA sequences (data not shown).

No amplification of target sequences was obtained from CSF- or LMD-derived DNA of patient 3 and 4 using primers targeting the fragments homologous to *Halobacterium* (data not shown).

DISCUSSION We report a new type of encephalomyelitis in 4 unrelated Japanese patients. All patients exhibited comparable clinical, radiologic, and histopathologic features, suggesting a shared pathogen. All inhabited a small Japanese island, but no direct person-to-person contact or other mode of transmission was identified; thus, we assumed that other people in this region may be exposed to the causative pathogen, but few are infected.

Progressive disease course, abnormal cytologic results, elevated CXCL13, and radiologic diversity suggested an infectious entity; however, common clinical features of infectious encephalitis, such as fever, increased number of WBCs in peripheral blood count, or elevation of C-reactive protein, were absent. Rather, slow progression and mild pathologic changes in the brain indicated a relatively moderate host immune response, indicative of the weak toxicity or virulence of the pathogen. In addition,

---

Figure 3   Stepwise strategy of bioinformatic analysis of sequencing results

Patient LMD DNA sample (PAS-positive lesions in biopsied brain tissue)

Total reads (patient 3 PAS+) N=7,292,715	Total reads (patient 4 PAS+) N=303,698
Map to human genome (using CLC Genomics Workbench)	Map to human genome (using CLC Genomics Workbench)
Mapped reads n=6,806,724 / Unmapped reads n=485,991	Mapped reads n=246,668 / Unmapped reads n=57,030
Map to human mRNA (Using CLC Genomics Workbench)	Map to human mRNA (Using CLC Genomics Workbench)
Mapped reads n=213,473 / Unmapped reads n=272,518	Mapped reads n=496 / Unmapped reads n=56,534
Map to nucleotide database (Using NCBI blastn: E-value ≤ 1e-20 hit length ≥ 80 base)	Map to nucleotide database (Using NCBI blastn: E-value ≤ 1e-20 hit length ≥ 80 base)
Reads of HALOBACTERIA n=130	Reads of HALOBACTERIA n=126

We obtained 7,292,715 and 303,698 DNA sequence reads from the affected brain tissues of patients 3 and 4, respectively. After trimming off low-quality sequence regions, we mapped them to the human genome and messenger RNA (mRNA) reference sequences using CLC Genomics Workbench. The 272,518 reads from patient 3 (3.7% of the total reads) and the 56,534 reads from patient 4 (18.6% of the total reads) that aligned with neither the human genome nor the mRNA reference sequences were further analyzed using BLASTN against the nucleotide database with a cutoff E-value of $<1e^{-20}$. LMD = laser microdissection; NCBI = National Center for Biotechnology Information; PAS = periodic acid-Schiff.

Hematoxylin & eosin staining (A), periodic acid-Schiff (PAS) staining (B), and Grocott staining (C) of brain biopsy samples show the presence of round pathogens, similar to Michaelis-Gutmann bodies, located mainly around the blood vessels. Some CD4-positive T lymphocytes are also located around the vessels (D). CD8-positive T lymphocytes appear to be the main invasive cells (E), whereas CD68-positive macrophages are only present in patches (F). Toluidine blue and Safranin O stain of Epon-embedded semithin sections show some pathogens without nuclei around vessels (G). Electron microscopy (H–J) shows an irregular shape of pathogens (diameter 2–7 mm) without cell walls and nuclei (arrows) but with some membranous structures in the cytoplasm (triangles). Scale bar 5 5 mm. Brain biopsies from patients 2 (K), 3 (L), and 4 (M) demonstrate a similar histopathology to that of patient 1, with 2–7 mm round PAS-positive pathogens located mainly around the vessels. The agents showed an irregular shape with no detectable cell wall or nucleus under an electron microscope (arrows). Scale bar 5 5 mm.

conditions E-value 1e^{-20}, hit length. 80, and identity . 70% (figure 3, table e-3). These sequences were not substantially homologous to known bacteria or eukarya sequences (E-value 1e^{-3}). Moreover, of 303,698 DNA fragments isolated from patient 4, 126 reads also showed a high degree of homology with Halobacteria, particularly *Halorubrum lacusprofundi* and *Halophilic archaea* (figure 3, table e-3). In contrast, genomic DNA extracted from brain tissues of patients with papillary meningioma (4,760,858 reads), intravascular lymphomatosis (5,259,934 reads), or glioblastoma (5,027,830 reads) showed no significant homology to known archaeal genomic or mRNA sequences (data not shown).

No amplification of target sequences was obtained from CSF- or LMD-derived DNA of patient 3 and 4 using primers targeting the fragments homologous to *Halobacterium* (data not shown).

We report a new type of encephalomyelitis in 4 unrelated Japanese patients. All patients exhibited comparable clinical, radiologic, and histopathologic features, suggesting a shared pathogen. All inhabited a small Japanese island, but no direct person-to-person contact or other mode of transmission was identified; thus, we assumed that other people in this region may be exposed to the causative pathogen, but few are infected. Progressive disease course, abnormal cytologic results, elevated CXCL13, and radiologic diversity suggested an infectious entity; however, common clinical features of infectious encephalitis, such as fever, increased number of WBCs in peripheral blood count, or elevation of C-reactive protein, were absent. Rather, slow progression and mild pathologic changes in the brain indicated a relatively moderate host immune response, indicative of the weak toxicity or virulence of the pathogen. In addition,

Stepwise strategy of bioinformatic analysis of sequencing results

We obtained 7,292,715 and 303,698 DNA sequence reads from the affected brain tissues of patients 3 and 4, respectively. After trimming off low-quality sequence regions, we mapped them to the human genome and messenger RNA (mRNA) reference sequences using CLC Genomics Workbench. The 272,518 reads from patient 3 (3.7% of the total reads) and the 56,534 reads from patient 4 (18.6% of the total reads) that aligned with neither the human genome nor the mRNA reference sequences were further analyzed using BLASTN against the nucleotide database with a cutoff E-value of , 1e^{-20}. LMD 5 laser microdissection; NCBI 5 National Center for Biotechnology Information; PAS 5 periodic acid-Schiff.

Neurology: Neuroimmunology & Neuroinflammation

Moreover, inhibition of cell wall synthesis by ceftriaxone induces morphologic alterations in common bacteria[11]; however, patients 3 and 4 were not treated with antibiotics before brain biopsy.

Unbiased high-throughput sequencing has proven effective for the identification of infectious pathogens.[12–14] Using this method, we successfully identified more than 100 sequences closely homologous to the genome of Halobacterial species from the DNA samples of 2 patients (table e-3). Therefore, we propose that this unknown pathogen genetically resembles *Halobacterium*, a genus of the domain Archaea. Based on unique ultrastructural features and sequence homology, we suggest that the causative pathogen is a *Halobacterium*. Unfortunately, no amplicon products were obtained from brain tissue or CSF of patients 3 and 4 using multiple archaeal universal primers or fragment-specific primers. This may be attributed to the low amount of target pathogen DNA obtained, the high mutation rate of the archaeal genome, or the lower sensitivity of nested PCR, which can lead to false-negative results.[15]

No evidence of CNS disorders due to archaeal infection has been reported. The domain Archaea, one of the 3 domains of living organisms together with eukarya and bacteria,[16] is a highly diverse and abundant group of prokaryotes usually inhabiting extreme environments such as salt lakes, deep seas, and hot springs.[14] They have also been detected in the human vagina, colon, and oral cavity.[17,18] In 2003, the pathogenicity and disease association of archaea were precisely forecasted.[19] Although the virulence of these organisms has not been confirmed, the relationship between the severity of periodontal disease and the abundance of archaeal rRNA in the subgingival crevice has been reported.[17]

Given the abundant evidence of an infectious entity, various antibiotics, including ampicillin, ceftriaxone, streptomycin, and minocycline, were administered, none of which proved effective. In contrast, TMP-SMX plus corticosteroids had a rapid curative effect in all 4 patients. TMP-SMX monotherapy did not produce a complete therapeutic effect, suggesting that an anti-inflammatory is also required.[9] We recommend a high dose of TMP-SMX (6–12 g/day) plus steroids as first-line treatment, as this regimen dramatically reversed symptoms in patients 1 and 3 without severe adverse events. However, patients 2 and 4 developed acute liver failure as a side effect of high-dose TMP-SMX, and neurologic symptoms gradually deteriorated upon TMP-SMX withdrawal. Patient 2 was then treated with lower-dose TMP-SMX intermittently for 5 years with substantial symptom improvement, whereas patient 4 deteriorated to a vegetative state and died despite reexposure to low-dose TMP-SMX (2 g/day) in combination with corticosteroids.

We attempted to cultivate the pathogen from the biopsied brain sample of patient 3 using a medium containing 15% or 20% NaCl under aerobic conditions. However, the cultivation was unsuccessful, possibly because our tissue preservation protocol may not be appropriate for organisms without cell walls, such as *Mycoplasma*, which are sensitive to mechanical stress.[20] In this study, the target pathogen could have been destroyed by mechanical stressors such as ice crystals because all biopsied brain samples were preserved without cryoprotectants.

We propose a new disease entity for infectious encephalomyelitis identified in 4 Japanese patients on the basis of the following criteria: (1) geographical clustering; (2) comparable clinical features, including progressive dementia with involuntary tongue movements; serum and CSF cytologic examination; similar lesion patterns on MRI; and sensitivity to TMP-SMX; and (3) unique ultrastructural characteristics of the undescribed pathogen. Using unbiased high-throughput sequencing, the potential pathogen was tentatively identified as a species of archaea, despite the subsequent unsuccessful genetic or cellular studies. As the next step, we need to clarify the pathogenicity of the PAS-positive agent by immunohistochemical studies using patient serum. Further experiments are required to validate archaea as the causative agent and to identify the specific species, natural host, route of transmission, pathogenic mechanism, and epidemiology. We recommend the application of high-dose TMP-SMX therapy to this encephalomyelitis. Our work will shed light on an undiagnosed encephalomyelitis.

REFERENCES

1. Costello DJ, Eichler FS, Grant PE, Auluck PK. Case records of the Massachusetts General Hospital. Case 1-2009. A 57-year-old man with progressive cognitive decline. N Engl J Med 2009;360:171–181.
2. Geschwind MD, Shu H, Haman A, Sejvar JJ, Miller BL. Rapidly progressive dementia. Ann Neurol 2008;64:97–108.
3. Yogi T, Hokama A, Kinjo F, et al. Whipple's disease: the first Japanese case diagnosed by electron microscopy and polymerase chain reaction. Intern Med 2004;43:566–570.
4. Uryu K, Sakai T, Yamamoto T, et al. Central nervous system relapse of Whipple's disease. Intern Med 2012; 51:2045–2050.
5. Yajima N, Wada R, Kimura S, et al. Whipple disease diagnosed with PCR using formalin-fixed paraffin-embedded specimens of the intestinal mucosa. Intern Med 2013;52: 219–222.
6. Yoshitake T, Kiyohara Y, Kato I, et al. Incidence and risk factors of vascular dementia and Alzheimer's disease in a defined elderly Japanese population: the Hisayama Study. Neurology 1995;45:1161–1168.
7. Chu AB, Sever JL, Madden DL, et al. Oligoclonal IgG bands in cerebrospinal fluid in various neurological diseases. Ann Neurol 1983;13:434–439.
8. Fenollar F, Puechal X, Raoult D. Whipple's disease. N Engl J Med 2007;356:55–66.
9. Schneider T, Moos V, Loddenkemper C, Marth T, Fenollar F, Raoult D. Whipple's disease: new aspects of pathogenesis and treatment. Lancet Infect Dis 2008;8: 179–190.
10. Yasuda M, Oyaizu H, Yamagishi A, Oshima T. Morphological variation of new Thermoplasma acidophilum isolates from Japanese hot springs. Appl Environ Microbiol 1995;61:3482–3485.
11. Ullmann U, Hammer-Uschtrin U. Influence of cefmenoxime, ceftriaxone, latamoxef, and ceftazidime on the lysis of Klebsiella pneumoniae: a light and electron microscopic study. Am J Med 1984;77:21–24.
12. Palacios G, Druce J, Du L, et al. A new arenavirus in a cluster of fatal transplant-associated diseases. N Engl J Med 2008;358:991–998.
13. Quail MA, Smith M, Coupland P, et al. A tale of three next generation sequencing platforms: comparison of Ion Torrent, Pacific Biosciences and Illumina MiSeq sequencers. BMC Genomics 2012;13:341.
14. Wilson MR, Naccache SN, Samayoa E, et al. Actionable diagnosis of neuroleptospirosis by next-generation sequencing. N Engl J Med 2014;370:2408–2417.
15. Kawada J, Kimura H, Ito Y, et al. Comparison of real-time and nested PCR assays for detection of herpes simplex virus DNA. Microbiol Immunol 2004;48: 411–415.
16. Woese CR, Kandler O, Wheelis ML. Towards a natural system of organisms: proposal for the domains Archaea, Bacteria, and Eucarya. Proc Natl Acad Sci USA 1990;87: 4576–4579.
17. Lepp PW, Brinig MM, Ouverney CC, Palm K, Armitage GC, Relman DA. Methanogenic Archaea and human periodontal disease. Proc Natl Acad Sci USA 2004;101:6176–6181.
18. Dridi B. Laboratory tools for detection of archaea in humans. Clin Microbiol Infect 2012;18:825–833.
19. Eckburg PB, Lepp PW, Relman DA. Archaea and their potential role in human disease. Infect Immun 2003;71: 591–596.
20. Kim KS, Clyde WA Jr, Denny FW. Physical properties of human Mycoplasma species. J Bacteriol 1966;92: 214–219.